https://dx.doi.org/10.21577/0103-5053.20220110

J. Braz. Chem. Soc., Vol. 34, No. 3, 309-324, 2023

Article

Inhibition of Copper Corrosion in Acid Medium by Imidazole-Based Compounds: Electrochemical and Molecular Approaches

Stefane N. Costa,[a] Francisco W. Q. Almeida-Neto,[b] Emmanuel S. Marinho,[c] Othon S. Campos,[d] Adriana N. Correia[b] and Pedro de Lima-Neto[,b]*

[a]*Programa de Pós-Graduação em Engenharia e Ciência de Materiais, Universidade Federal do Ceará, Campus do Pici, 60440-554 Fortaleza-CE, Brazil*

[b]*Departamento de Química Analítica e Físico-Química, Universidade Federal do Ceará, Campus do Pici, 60440-900 Fortaleza-CE, Brazil*

[c]*Faculdade de Filosofia Dom Aureliano Matos, Universidade Estadual do Ceará, 62930-000 Limoeiro do Norte-CE, Brazil*

[d]*Departamento de Química e Física, Universidade Federal do Espírito Santo, Campus Guararema 29500-000 Alegre-ES, Brazil*

Chemically modified imidazole molecules: 4-(1*H*-imidazol-1-yl)aniline, 4-(1*H*-imidazol-1-yl)benzaldehyde, 4-(1*H*-imidazol-1-yl)phenol and (4-(1*H*-imidazol-1-yl)phenyl)methanol were investigated as inhibitors of the copper (Cu^0) corrosion in 0.5 mol L^{-1} H_2SO_4 medium. The electrochemical corrosion data were obtained by monitoring open circuit potential, linear potentiodynamic polarization and electrochemical impedance spectroscopy techniques, while the computational density functional theory (DFT) method was applied to correlate the electronic properties of the molecules with corrosion inhibition efficiencies. All molecules had inhibited the Cu corrosion, and the inhibition values lied between 80 and 94%. A good correlation between the inhibition efficiencies values and Gibbs adsorption energy was found, showing that the more negative Gibbs energy, better interaction between the corrosion inhibitor with the Cu^0 surface, diminishing its corrosion in 0.5 mol L^{-1} H_2SO_4 medium. The DFT calculations showed significative differences in electronic and reactivity properties of imidazole and other molecules. The higher corrosion inhibition of imidazole derivates could be explained by electrophilic characteristic of these molecules, since there are empty molecular orbitals spread over mainly in benzene rings that make a metal-ligand charge transfer, receiving electronic density from the copper surface by backbonding, according to the electronic Fukui functions and the potential charge distribution considering the map of electrostatic potential.

Keywords: corrosion inhibitors, imidazole derivatives, density functional theory, copper, H_2SO_4

Introduction

The corrosion of materials, specifically the metallic ones, is one of the major problems faced by humankind, which lead to huge economic losses that also contributes to environmental pollution.[1] Cu^0 is one of those metallic materials that has been widely used in industries, having many technological applications due to its high electrical and thermal conductivity, good malleability and excellent corrosion resistance.[2] However, when Cu^0 is attacked by hydrochloric and sulfuric acids, which are frequently used in pickling industrial processes, can suffer dissolution in these aggressive media.[3]

For preventing metallic corrosion, one of the most applied methods is the use of organic or inorganic compounds as corrosion inhibitors.[4] Regarding of organic substances, the corrosion inhibition usually happens based on the adsorption of the molecule over the surface of the metallic materials through heteroatoms, such as nitrogen (N), oxygen (O), sulfur (S) and phosphorus (P), in addition to multiple bonds or aromatic rings.[5]

Several types of substances are being investigated as potential corrosion inhibitors for Cu^0, such as: azoles,[6] amines,[7] amino acids,[8] thiazoles,[9] pyrimidine[10] and Schiff's base.[11] In addition to having interesting

*e-mail: pln@ufc.br
Editor handled this article: Rodrigo A. A. Muñoz (Associate)

chemical and pharmacological properties, imidazole-based compounds have aromatic heterocyclic containing heteroatoms (N), which contribute to the adsorption of these species on the metal surface.[12,13] Although imidazole (IM) itself is not a promising corrosion inhibitor,[12,14] the corrosion inhibition efficiency (ε_{inh}) increases when polar chemical groups are added to the IM, such as phenyl, methoxy, amine, sulfhydryl, etc.[15] This is attributed to the heteroatoms of these substituents which tend to create a coordination compound between the corrosion inhibitor and the metallic surface, improving the adsorption of molecules on the metal surface.[16] In this context, the understanding of the interactions between the corrosion inhibitor and the metallic surface at a microscopic level has great importance for corrosion inhibition researchers, since one knows which molecular or electronic properties could be related to corrosion inhibition, making possible to correlate the calculated molecular properties with experimental data, such as ε_{inh}, for proposing chemical modifications of the molecule to synthesize new molecules with better corrosion inhibition performance.[17] In recent years, the so-called computational chemistry has been present in research not only on the subject of corrosion inhibitors, but also in the chemistry of materials such as the use of machine learning tools to study failures in metallic structures[18] or even using the *ab initio* method based on density functional theory (DFT) methodology, which uses quantum mechanics to determine molecular properties to evaluate macroscopic phenomena such as adsorption of inhibitor at the electrode/solution interface.[19] Thus, the correlation between experimental results and theoretical calculations allows to deepen the physical and chemical understandings of the phenomenon of corrosion inhibition.[20]

Therefore, the aim of this investigation is the application of imidazole-based compounds towards Cu^0 corrosion inhibition in acidic medium and correlating these experimental data with *in silico* analysis of the inhibitor molecules by using DFT methods.

Experimental

Chemicals

All chemicals were purchased from Sigma-Aldrich Brazil (Barueri, Brazil) and used as received, without any further purification or separation. The 2D representations of investigated molecules are shown in Figure 1.

Electrochemical experiments

Electrochemical techniques, such as open circuit potential monitoring (E_{oc}), potentiodynamic polarization (PP) and electrochemical impedance spectroscopy (EIS), were used to assess the performance of the imidazole and its derivatives as inhibitors of the Cu^0 corrosion in 0.5 mol L^{-1} H_2SO_4. All electrochemical experiments were carried out in a conventional three-electrode connected to Autolab PGSTAT 302N potentiostat/galvanostat from Metrohm® (Utrecht, The Netherlands) and controlled by Metrohm® NOVA® 2.1.4 software (Utrecht, The Netherlands), which allows the acquisition of experimental data and further treatment and analysis. The working electrode was a Cu^0 disk embedded in glass tubes with epoxy resin and with a disk exposed area of approximately 0.18 cm^2. The counter electrode was a platinum plate with an area of 1.13 cm^2 and the reference electrode was $Ag_{(s)}/AgCl_{(s)}/Cl^-$ (aq., saturated KCl). All solutions used in this investigation were prepared by water purified by the Milli-Q system (Darmstadt, Germany).

Prior the electrochemical corrosion tests, the Cu^0 surface was submitted to a sanding process with silicon

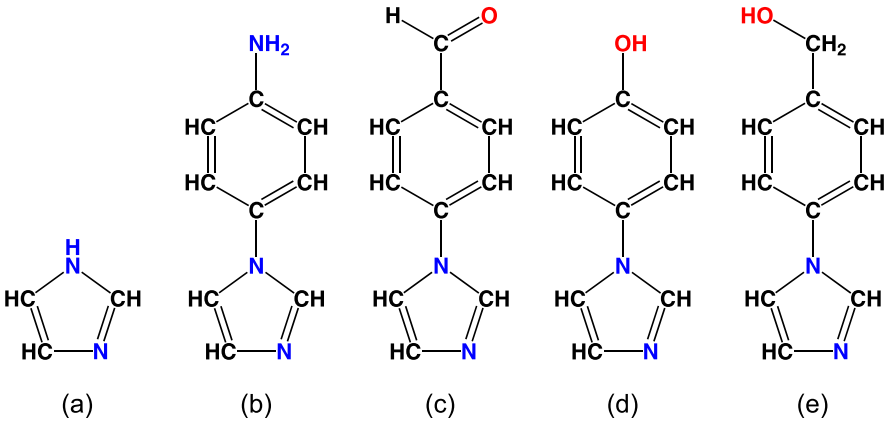

Figure 1. 2D chemical representations of imidazole (IM) (a), 4-(1*H*-imidazol-1-yl)aniline (IA) (b), 4-(1*H*-imidazol-1-yl)benzaldehyde (IB) (c), 4-(1*H*-imidazol-1-yl)phenol (IF) (d) and (4-(1*H*-imidazol-1-yl)phenyl)methanol (IFM) (e).

carbide (SiC) sandpapers with 100, 220, 400 and 600 mesh granulations. After, the Cu^0 surface was washed with water. Finally, the samples were immersed in a 0.5 mol L^{-1} H_2SO_4 aerated solution and in the absence (blank solution) and presence of the imidazole-based compounds in the following concentrations: 0.1×10^{-3}, 0.25×10^{-3}, 0.5×10^{-3} and 1×10^{-3} mol L^{-1}.

The impedance data were obtained at E_{oc} and after 1 h of immersion of the Cu^0 in the testing solution. The frequency was ranged between 20 kHz to 6 mHz and a potential amplitude of 10 mV was applied. The PP curves were obtained at the concentration of 1×10^{-3} mol L^{-1}, after 1 h of immersion time, and the potential was sweep between ± 300 mV around the E_{oc} value, and the scan rate used was 1 mV s^{-1}. All electrochemical experiments were carried out at the laboratory room temperature (ca. 25 °C) in triplicate.

Computational calculations

The input files were prepared using the GaussView 5.0[21] software and all the calculations were done using the Gaussian 09 software.[22] Since the acidic medium was used in the experimental tests, the DFT calculations were carried out considering that all molecules were protonated. To make a proper theoretical-experimental model, the inhibitors molecules were optimized using the Minnesota 06 hybrid meta exchange-correlation functional (M06-2X) with the 6-311++G(d,p) basis set.[23,24] All molecules were submitted for calculation with water as implicit solvent by the solvation method IEF-PCM.[25,26] The isosurfaces of the frontier molecular orbitals (FMO) were rendered using the trial version of the ChemCraft software.[27] Then, the global quantum reactivity descriptors were calculated from the energy values of the highest occupied molecular orbital (HOMO) and lowest unoccupied molecular orbital (LUMO): the energy gap (ΔE_{gap}, equation 1),[28] the ionization potential (IP, equation 2),[29] the electron affinity (A, equation 3),[29] the electronegativity (χ, equation 4),[30,31] the global hardness (η, equation 5),[32-34] the global softness (S, equation 6),[35] the global electrophilicity index (ω, equation 7),[36] the global nucleophilicity index (ε, equation 8),[37] and the fraction of electrons transferred (ΔN, equation 9).[38] For the Cu metallic bulk, it can be classified as soft ($\eta_M = 0$)[39] and its electronegativity (χ_M) has the value of 4.68 eV.[40] Finally, to create a local reactivity characterization map, the electronic Fukui functions for the nucleophilic (f^+) and the electrophilic (f^-) attack obtained from the Multiwfn software[41] and the molecular electrostatic potential (MEP) were calculated using the M06-2X/6-311++G(d,p) computational level and the isosurfaces were rendered by the VESTA[42] and Gabedit[43] software respectively.

$$\Delta E_{gap} = E_{LUMO} - E_{HOMO} \quad (1)$$

$$IP = -E_{HOMO} \quad (2)$$

$$A = -E_{LUMO} \quad (3)$$

$$\chi = \frac{I + A}{2} \quad (4)$$

$$\eta = \frac{I - A}{2} \quad (5)$$

$$S = \frac{1}{\eta} \quad (6)$$

$$\omega = \frac{\chi^2}{2\eta} \quad (7)$$

$$\varepsilon = \frac{1}{\omega} \quad (8)$$

$$\Delta N = \frac{\chi_M - \chi_{Inh}}{2(\chi_M + \chi_{Inh})} \quad (9)$$

Results and Discussion

Electrochemical studies

Figure 2 shows the evolution of the E_{oc} values with the immersion time of the Cu electrode in 0.5 mol L^{-1} H_2SO_4 solution. Considering the blank solution, the E_{oc} values showed a slightly shift towards more negative potential (from 27 to 19 mV), followed by the formation of a potential plateau after 900 s. For other solutions containing imidazole-based compounds, the Cu^0 electrode

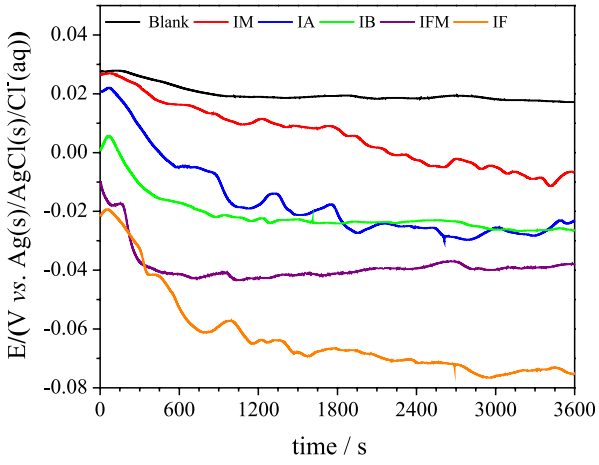

Figure 2. Variation of the open circuit potential with the immersion time of Cu^0 in 0.5 mol L^{-1} H_2SO_4. These measurements were carried out at laboratory room temperature (ca. 25 °C) and in the presence and absence (blank) of imidazole-based compounds at 1×10^{-3} mol L^{-1}.

displayed more negative E_{oc} values compared with its E_{oc} values shown in the blank solution. Furthermore, it can be noted that for all investigated corrosion inhibitors, the E_{oc} values shift towards more negative, and the stabilization period of 1 h was enough to reach a steady state.[44] The E_{oc} monitoring shows that imidazole and their derivatives probably have a greater inhibitory effect on the cathodic reaction than the anodic reaction of the Cu^0 corrosion.[45] This phenomenon is explained by the adsorption of the imidazole-based molecules on the active sites on the Cu^0 surface, changing the oxygen concentration at the electrode/solution interface.[45-47]

Potentiodynamic polarization curves obtained for Cu^0 in aerated 0.5 mol L^{-1} H_2SO_4 solution in the presence and absence of the imidazole-based compounds are shown in Figure 3. Figure 3a shows that the corrosion potentials (E_{corr}) for imidazole-based compounds are shifted towards more negative values in comparison to the blank curve, as seen in Figure 2. In addition, the cathodic branches of all curves showed a tendency to reach a current density plateau, indicating that the predominant cathodic reaction on Cu^0 surface in H_2SO_4 medium is the oxygen reduction reaction (ORR).[48] Thus, the shifting of the E_{corr} towards more negative values in the presence of the imidazole-based compounds was attributed to the inhibition of the ORR related to the adsorption of the investigated molecules blocking the cathodic sites of Cu^0 electrode.

Two distinct regions (from 0.0 to 0.15 V and from 0.15 to 0.30 V) can be seen in the anodic branch from blank solution (Figure 3) which suggest that Cu^0 corrodes in aerated 0.5 mol L^{-1} H_2SO_4 by two different dissolution pathways through two intermediates, Cu^I_{ads} and Cu^{II}_{ads}, as described by Cordeiro *et al.*[49] The mechanism proposed by Cordeiro *et al.*[49] is described by the electrochemical reactions displayed in equations 10 to 13. According to this mechanism, near the corrosion potential only Cu^I_{ads} species are present and the copper electrodissolution occurs via k_2. For higher anodic overpotentials the second electrodissolution path (k_4) becomes important and Cu^{II}_{ads} species predominates on the copper surface. Finally, since the electrochemical impedance measurements were obtained at open circuit potential, we will consider the dissolution to Cu^{II}_{sol} only through Cu^I_{ads} (k_2), followed by its diffusion to the solution.

The addition of all corrosion inhibitors decreased the anodic density current. Initially, there is the formation of the cuprous ion on the Cu^0 surface (Cu^I_{ads}, equation 10), which is adsorbed on the surface of the electrode as described by Cordeiro *et al.*[49] In the absence of the imidazol-based compounds, Cu^I ion is oxidized to cupric ion (Cu^{II}), followed by its diffusion to the solution (equation 11). In presence of the imidazole-based molecules, the Cu^I_{ads} ion reacts with the inhibitor (I_{nh}) to form a complex film adsorbed on the Cu^0 surface (equation 14), which acts as a physical barrier that alters the Cu^0 dissolution kinetics, causing the non-occurrence of the Tafel's relationship in the anodic curves. Finally, the Figure 3b shows that the both values of the cathodic and anodic current densities obtained in the presence of the corrosion inhibitors are smaller compared to those obtained in the absence of the imidazole derivatives, showing that both ORR and Cu^0 dissolution are inhibited by the studied imidazole-based compounds.

$$Cu \underset{k_{-1}}{\overset{k_1}{\rightleftharpoons}} Cu^I_{ads} + e^- \quad (10)$$

$$Cu^I_{ads} \xrightarrow{k_2} Cu^{II}_{sol} + e^- \quad (11)$$

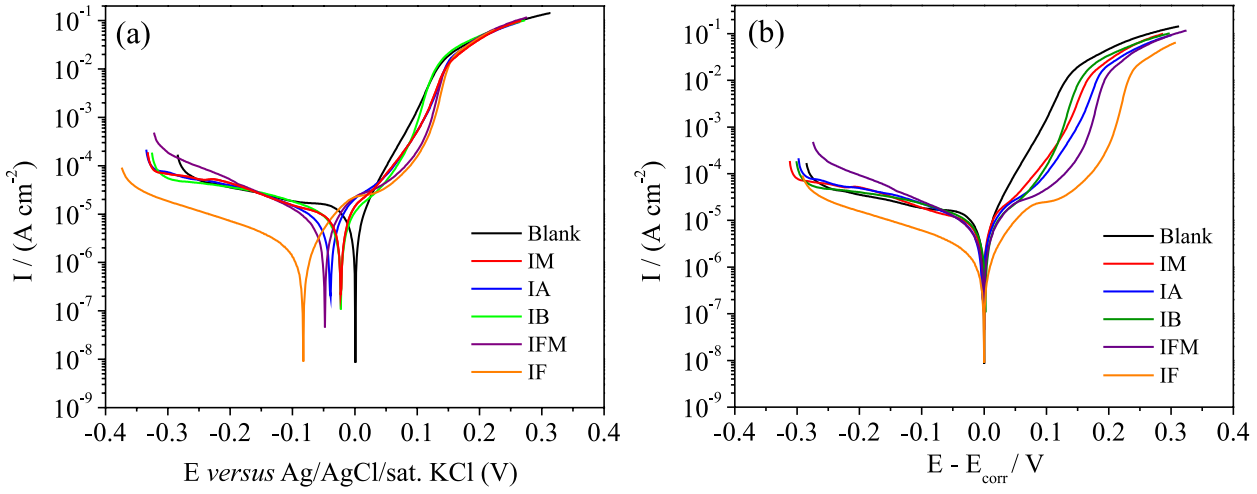

Figure 3. (a) Potentiodynamic polarization curves obtained for Cu^0 in 0.5 mol L^{-1} H_2SO_4 medium in the absence (blank) and presence of imidazole-based compounds at 1×10^{-3} mol L^{-1}. (b) The obtained cathodic and anodic current densities are plotted *versus* corrosion overpotential. All curves were achieved at laboratory room temperature (ca. 25 °C).

$$Cu^{I}_{ads} \underset{k_{-3}}{\overset{k_3}{\rightleftharpoons}} Cu^{II}_{ads} + e^- \quad (12)$$

$$Cu + Cu^{II}_{ads} \xrightarrow{k_4} Cu^{II}_{sol} + Cu^{I}_{ads} + e^- \quad (13)$$

$$Cu^{I}_{ads} + Inh^{I}_{sol} \rightarrow [Cu\text{-}Inh]^{II}_{ads} \quad (14)$$

Since Tafel extrapolation method cannot be applied to determine the corrosion current, the ε_{inh} values were calculated from the polarization resistance (R_p) values derived from the potentiodynamic polarization curves using the equation 15.[50] In this equation, R_p^0 is the polarization resistance obtained from blank solution and R_p is the corresponding value obtained from the solutions containing the imidazole-based molecules.

$$\varepsilon_{inh} = \left(1 - \frac{R_p}{R_p^0}\right) \times 100 \quad (15)$$

The corrosion parameters calculated from mathematical analyses of the potentiodynamic polarization curves are displayed in Table 1. Regarding E_{corr} values, all potential shifts were lower than 85 mV, which can classify imidazole and its derivatives as mixed inhibitors with cathodic efficiency predominantly.[51] According to the R_p values, it is possible to verify that imidazole and its derivatives favored the inhibition of Cu^0 dissolution and that the ε_{inh} followed the following sequence: 4-(1*H*-imidazol-1-yl) phenol (IF) > (4-(1*H*-imidazol-1-yl)phenyl)methanol (IFM) > 4-(1*H*-imidazol-1-yl)benzaldehyde (IB) > 4-(1*H*-imidazol-1-yl)aniline (IA) > imidazole (IM). Therefore, all imidazole-based molecules are more efficient in the inhibition of the Cu^0 dissolution compared to the imidazole molecule.

To obtain more information regarding the behavior of inhibitors on the surface of the Cu^0 electrode, EIS measurements were performed in 0.5 mol L^{-1} H_2SO_4 medium, in the absence and presence of imidazole derivatives at 1×10^{-3} mol L^{-1}, as shown in Figure 4. In Figure 4a, it is possible to observe that all Nyquist curves show one capacitive semicircle at high-frequency region, followed by a straight line at low-frequency region.[52] This straight line is known as Warburg impedance, and it could be associated with the ORR due to the diffusion of the dissolved gas from the solution to the Cu^0 surface[53] and to the diffusion of the Cu^{II} species towards the solution. Since the oxygen dissolved in the electrolyte interacts with Cu^0 surface, there is an adsorption of the oxygen molecules on the active sites of the electrode. In this context, there is a competition between oxygen gas and inhibitor molecule by the surface of the electrode, and the capacitive arcs achieved for the imidazole and all imidazole derivatives are larger compared to that obtained in the absence of these molecules, indicating that all tested molecules promoted an increase in the charge transfer resistance of the Cu^0 dissolution. The adsorption of the corrosion inhibitors on the Cu^0 surface becomes a barrier that lead to the inhibition of its dissolution kinetics by the blockage of the anodic active sites.[54]

Figures 4b and 4c shows the typical Bode plots obtained for the studied systems. In Figure 4b, it can be noted that in presence of the corrosion inhibitors, impedance modules increased by one order of magnitude in the low-frequency region compared to the blank solution, confirming that the derivatives are efficient against Cu^0 corrosion in the H_2SO_4 medium.[55] In addition, in Figure 4c, all phase angles plots display a maximum extended of approximately 80° in the high frequency region, suggesting the formation of a layer on the Cu^0 surface.[48,56]

Since the capacitive arcs observed in the Nyquist diagrams (Figure 4a) are related with two coupled processes, the equivalent electric circuit, shown in Figure 5, was used to fit all impedance data.[57-62] In this circuit, R_1 is the resistance of the solution, R_2 is the resistance of the chemical species adsorbed on the Cu^0 surface, R_3 is the charge transfer resistance; W is the Warburg impedance; Q_1 is the element film phase constant, and Q_2 is the double layer phase constant element.[56] The phase constant element (Q) was used to replace the capacitance in the equivalent electrical circuits, since the surface presents irregularities or roughness due to Cu^0 surface sanding.[63] All impedance parameters derived from equivalent electric circuit analyses are listed in Table 2 and the ε_{inh} values were calculated according to equation 15, where R_p^0 ($R_p^0 = R_2^0 + R_3^0$) is the polarization resistance obtained from the blank solution, while R_p ($R_p = R_2 + R_3$) is the polarization resistance in the presence of the inhibitor.

Table 1. Electrochemical parameters obtained from the potentiodynamic polarization curves for Cu^0 corrosion in 0.5 mol L^{-1} H_2SO_4 medium in the absence and presence of imidazole-based compounds at 1×10^{-3} mol L^{-1}

	E_{corr} / mV	R_p / (kΩ cm^2)	ε_{inh} / %
Blank	0.08 ± 0.01	10.91 ± 0.19	–
IM	–22 ± 0.01	16.58 ± 0.12	52.04 ± 0.09
IA	–39 ± 0.02	19.47 ± 0.09	78.57 ± 0.02
IB	–22 ± 0.03	19.54 ± 0.11	79.21 ± 0.05
IFM	–50 ± 0.01	19.85 ± 0.04	82.05 ± 0.03
IF	–86 ± 0.02	21.17 ± 0.07	94.07 ± 0.10

E_{corr}: corrosion potential; R_p: polarization resistance; ε_{inh}: inhibition efficiency; IM: imidazole; IA: 4-(1*H*-imidazol-1-yl)aniline; IB: 4-(1*H*-imidazol-1-yl)benzaldehyde; IF: 4-(1*H*-imidazol-1-yl)phenol; IFM: (4-(1*H*-imidazol-1-yl)phenyl)methanol.

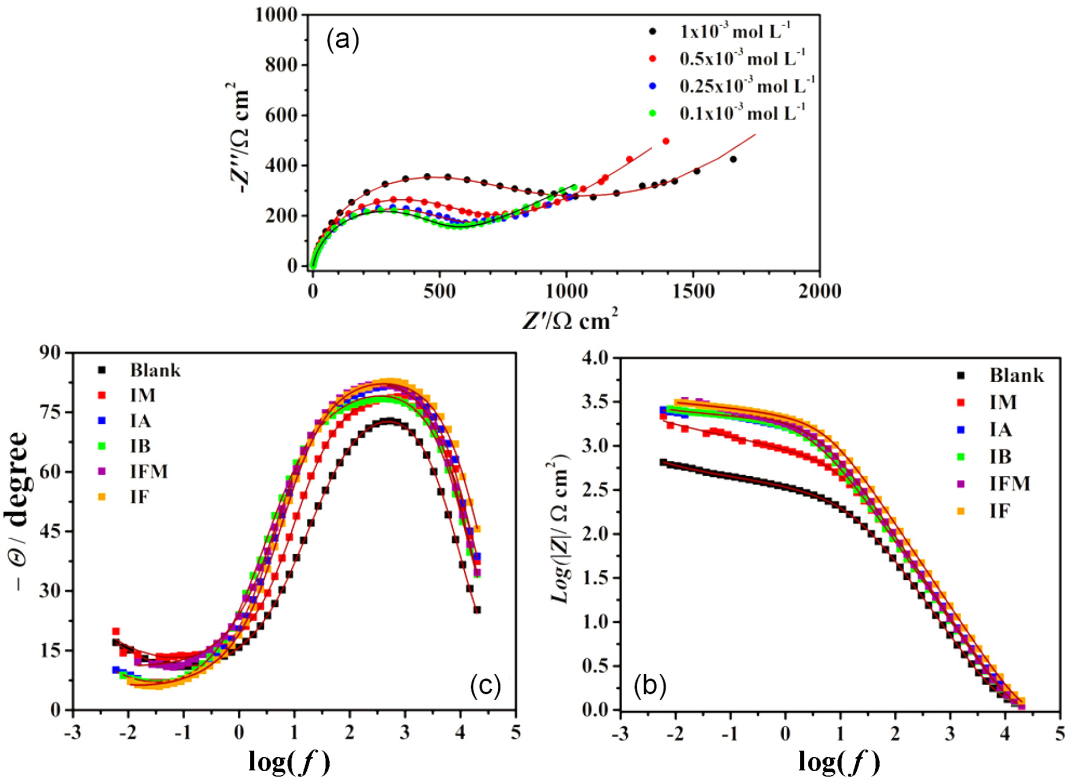

Figure 4. Nyquist (a) and Bode (b,c) plots obtained for Cu^0 after 1 h of immersion in 0.5 mol L^{-1} H_2SO_4 in the absence and presence of imidazole and its derivatives at 1×10^{-3} mol L^{-1}. All diagrams were obtained at room temperature of the laboratory (ca. 25 °C). The solid lines represent impedance simulation carried out by the equivalent circuit shown in Figure 5.

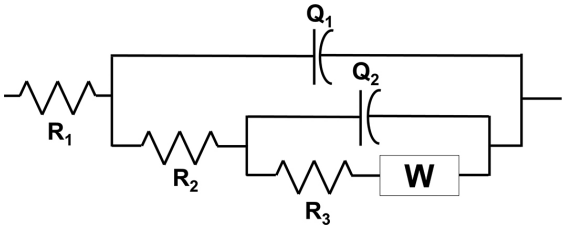

Figure 5. Drawing of the equivalent electrical circuit used to fit the EIS diagrams.

Table 2 shows a significant increase in R_2 values for all imidazole derivatives, confirming that the adsorption of compounds on the Cu^0 surface prevents the charge transfer process.[63-65] Since R_2 represents the double layer resistance from electrode/solution interface, Q_1 also represents the charge distribution in this region. Aiming a better representation for constant phase data, the Hsu and Mansfeld[64] and Brug *et al.*[65] models for pseudocapacitance conversion were applied for Q_1 and Q_2 values to, respectively, C_1 and C_2 values, as shown in equations 16-17.[64,65] In these equations, the resistance of the electrolyte (R_1), the charge transfer resistance of the Cu^0 electrode (R_2), the admittance values (Y_o) of Q_1 and n correspond to the values derived from the electrochemical fit.

$$C_1 = Y_0^{1/n} R_1^{1-n/n} \quad (16)$$

$$C_2 = Y_0^{1/n} \left(\frac{R_1 \times R_2}{R_1 + R_2} \right)^{\frac{1-n}{n}} \quad (17)$$

In addition, Table 2 also shows that the R_2 values increased in the following order: IM < IA < IB < IFM < IF, while R_3 values do not followed any trend. Moreover, C_1 and C_2 followed an inverse trend of charge density. This behavior can be attributed to the replacement of H_2O molecules on the electrode surface by molecules of imidazole derivatives.[66] In addition, the diffusion impedance fitted from Warburg element circuit decreased in the same trend from R_2. This effect suggests a blockage of the active surface area of Cu^0 electrode, and the modified imidazole molecules diminishes the Cu^{II} diffusion towards solution and that also hinders the oxygen adsorption on Cu^0 surface. The classical Warburg semi-infinite diffusion depends upon the surface coverage, as shown in equations 18 and 19.[67]

$$Z_{diff} = \sigma \tau^{-1/2} (1 - j) \quad (18)$$

In equation 18, Z_{diff} is the impedance of the Warburg element, σ is the Warburg coefficient τ is the applied frequency and j is equal to $-1^{1/2}$. The Warburg coefficient for a particular situation which the diffusion of reduced

Table 2. Fitted values obtained from the analyses of impedance diagrams, shown in Figure 4, using the equivalent electric circuit shown in Figure 5. The corrosion inhibition efficiency values obtained from the fitted data are also listed. The constant phase element was converted to pseudocapacitance using Brug method

Inhibitor	R_2[a] / (Ω cm^2)	C_1[b] × 10^7 / (F cm^{-2})	R_3[c] / (Ω cm^2)	C_2[d] × 10^7 / (F cm^{-2})	W_{diff}[e] / (Ω cm^2)	ε_{inh}[f] / %
Blank	367.72 ± 1.86	2.04 ± 0.97	132.24 ± 7.90	1.99 ± 0.23	3.20 ± 0.02	–
IM	936.44 ± 7.20	8.90 ± 2.47	64.10 ± 4.27	8.92 ± 5.54	2.54 ± 0.04	50.03
IA	1868.22 ± 4.79	4.59 ± 0.17	363.60 ± 24.18	4.44 ± 0.28	1.58 ± 0.01	77.60
IB	2127.63 ± 4.23	3.32 ± 0.89	289.38 ± 23.30	3.28 ± 0.26	1.57 ± 0.03	79.32
IFM	2175.60 ± 9.41	4.61 ± 0.41	277.47 ± 7.01	4.54 ± 0.49	1.13 ± 0.09	79.62
IF	2281.86 ± 7.64	4.30 ± 0.04	353.02 ± 9.71	4.22 ± 0.36	1.02 ± 0.01	81.03

[a]Charge transfer element for R_2; [b]pseudocapacitance from double layer; [c]charge transfer element for R_3; [d]pseudocapacitance for electrode surface; [e]diffusion impedance; [f]inhibition efficiency. IM: imidazole; IA: 4-(1*H*-imidazol-1-yl)aniline; IB: 4-(1*H*-imidazol-1-yl)benzaldehyde; IF: 4-(1*H*-imidazol-1-yl)phenol; IFM: (4-(1*H*-imidazol-1-yl)phenyl)methanol.

and oxidized species is the same is shown in equation 19.

$$\sigma = \frac{RT}{A_s F^2 \sqrt{2DC}} \frac{1}{\theta} \quad (19)$$

In equation 19, R is the universal gas constant, T the absolute temperature, A_s the active electrode area, F the Faraday's constant, C the concentration of the electrochemical species, D the diffusion coefficient and θ the surface coverage of the electrode. Since the Warburg coefficient is inversely proportional to the surface coverage, this means that the increase of the surface coverage by the inhibitors molecules leads to a decreased the corresponding σ values and, consequently, the diminishing of Z_{diff} occurs due to σ decrease. For instance, the equivalent impedance equation for this electrochemical system is shown in equation 20, which represents the equivalent impedance equation for the electric circuit shown in Figure 5.

When $Z_{diff} \rightarrow 0$, $\frac{1}{R_3 + Z_{diff}} \rightarrow \frac{1}{R_3}$, and Z_{eq} equation tends to be like a double RC equivalent circuit equation, given by equation 21:

$$Z_{eq} = R_1 + \frac{1}{j\omega C_1 + \frac{1}{R_p}} + \frac{1}{j\omega C_2 + \frac{1}{R_3 + Z_{diff}}} \quad (20)$$

$$Z_{eq} = R_1 + \frac{1}{j\omega C_1 + \frac{1}{R_2}} + \frac{1}{j\omega C_2 + \frac{1}{R_3}} \quad (21)$$

In an electrochemical application of equation Z_{eq} in the presented electrochemical cell, the corrosion of Cu^0 in H_2SO_4 0.5 mol L^{-1} solution is inhibited by all investigated molecules and, consequently, the diffusion of Cu^{II} ions do not occur due to the formation of the $[Cu\text{-}InH]^{II}_{ads}$ film on the Cu^0 surface, which is contrary to what happens in the absence of inhibitors, as it is better indicated in the corresponding plots shown in Figure 3. In this context, the Bode plots for modified imidazole molecules tends to behavior like a pure resistor, in contrast with blank solution, as shown in Figure 4b. This behavior agrees with literature showing the effect of inhibitor adsorption over the electrode surface, which hinders the diffusion of Cu^{II} ions to the bulk solution.[61] The ε_{inh} was calculated from equation 15 and the obtained values are listed in Table 2, which range from about 50% for the IM up to about 81% IF. Thus, as well as the inhibition efficiency determined by the PP technique, the EIS technique presented the same sequence as: IF > IFM > IB > IA > IM.

Adsorption isotherms

To understand the nature of adsorption process of the inhibitors, EIS measurements were performed with the variation of the concentration for imidazole and its derivatives and the obtained Nyquist plots are shown in Figure 6. In addition, EIS parameters derived from these Nyquist diagrams using the equivalent electric circuit, shown in Figure 5, are displayed in Table 3.

It can be seen in Table 3 that the polarization resistance presents a gradual increase as the concentration of inhibitors increases in the solution. Moreover, the surface coverage (θ), calculated from equation 22, increases as the inhibitor concentration also increased. Thus, the Langmuir isotherm model[68] was applied according the equation 23. In equation 22, C_{Inh} is the inhibitor concentration and K_{ads} is the equilibrium constant for the adsorption/desorption process. The isotherm plots of the studied corrosion inhibitors are shown in Figure 7.

$$\theta = \left(\frac{R_p - R_p^0}{R_p} \right) \quad (22)$$

$$\left(\frac{C_{Inh}}{\theta} \right) = C_{Inh} + \left(\frac{1}{K_{ads}} \right) \quad (23)$$

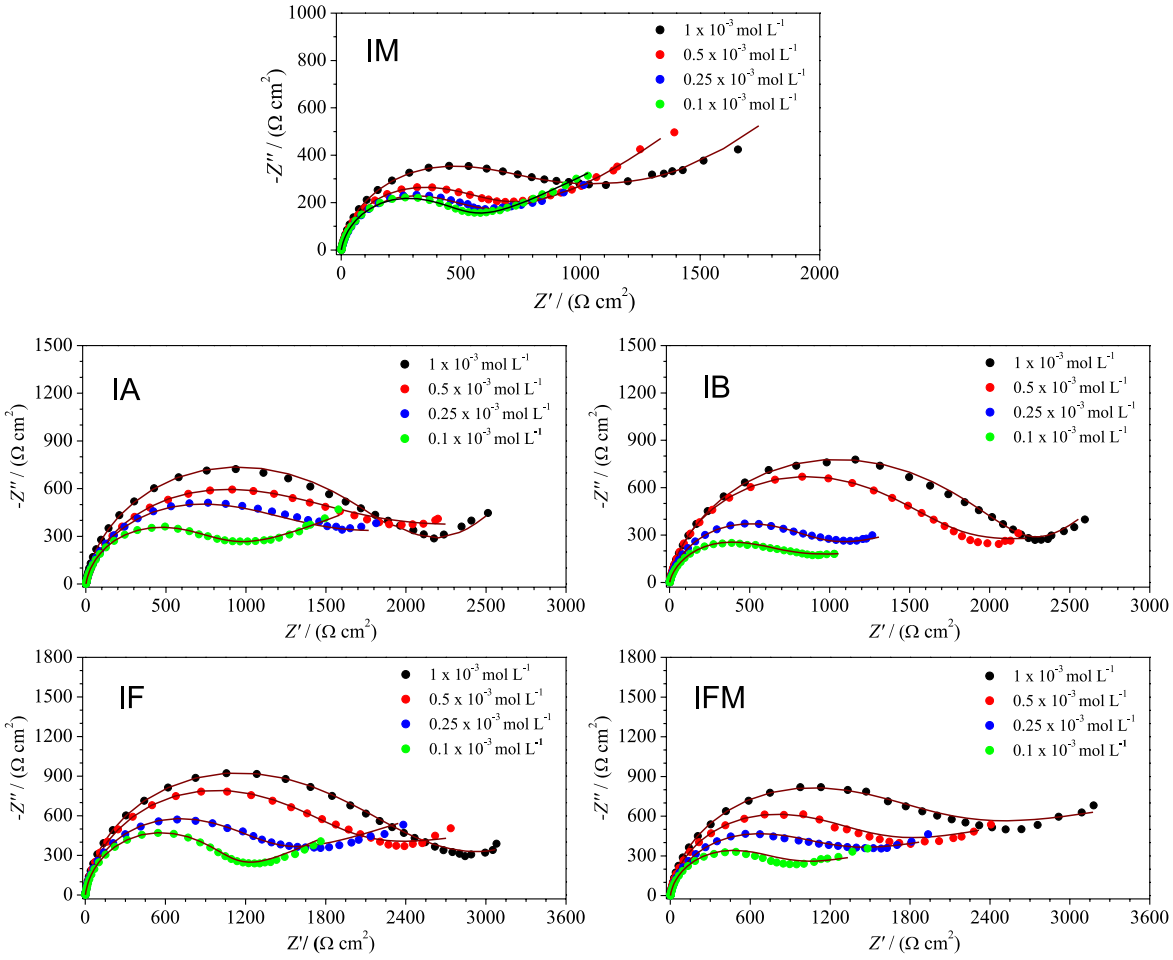

Figure 6. Nyquist diagrams obtained for Cu^0 immersed in 0.5 mol L^{-1} H_2SO_4 at different concentrations of the studied corrosion inhibitors and obtained at room temperature (ca. 25 °C). The solid lines represent the adjust of the experimental data by the equivalent electric circuit shown in Figure 5.

As can be seen in Figure 7, all isotherms are linear, which indicates that the inhibitors formed a monolayer on the substrate surface, effectively reducing the corrosion rate.[56] This gives us the information that each active site is occupied by only one molecule of the derivatives that do not interact with each other.[69] Except for imidazole molecule, the adsorption isotherms obtained for the modified imidazole compounds have similar angular coefficient and intercept. From Langmuir boundary conditions, the adsorption sites are unique and individual for each molecule, and the adsorbate will not interact laterally with other adsorbent sites. Therefore, the Langmuir model indicates that modified imidazole molecules had the same adsorption behavior. On the other hand, the modified imidazole molecules have different lateral groups, therefore, it is expected the existence of lateral interactions between the adsorbed molecules, which is not taken in consideration in the Langmuir model. Thus, the Frumkin isotherm model[70] was applied using equation 24 to evaluate the lateral interaction between the corrosion inhibitors molecules adsorbed on Cu^0 surface, and the isotherm plots for each investigated corrosion inhibitor molecule are shown in Figure 8. In equation 24, b is an intermolecular factor taken from experimental data,

$$K_{ads} C_{Inh} = \frac{\theta}{1-\theta} \exp(-2b\theta) \quad (24)$$

From Figure 8, it can be observed that for the Frumkin model, all isotherms are linear, and, except for the IM molecule, all the other molecules presented a positive slope, which is characteristic of lateral attractions during the adsorption process, while a negative slope stands for lateral repulsion between the adsorbed molecules,[71,72] and Table 4 shows the fitted intermolecular factor changes regarding the molecular modification of imidazole molecule.

The molecular modification of the imidazole molecule brought the capacity of lateral interactions due to both polar and non-polar groups, which increased the capacity of those molecules to create a protective layer in the copper electrode in acidic medium and the decrescent order of the intermolecular factor is: IF > IA > IFM > IB > IM. Since

Table 3. EIS parameters derived from the Nyquist plots, shown in Figure 6, using the equivalent electric circuit shown in Figure 5

	$C_{Inh} \times 10^{-3}$ / (mol L^{-1})	R_P / (Ω cm^2)	θ
Blank	–	499.95 ± 0.19	–
IM	0.10	537.10 ± 0.11	0.07 ± 0.02
	0.25	599.30 ± 0.09	0.17 ± 0.04
	0.50	713.56 ± 0.12	0.30 ± 0.08
	1.00	1000.56 ± 0.13	0.50 ± 0.03
IA	0.10	935.98 ± 0.05	0.47 ± 0.01
	0.25	1380.96 ± 0.12	0.64 ± 0.10
	0.5	1774.65 ± 0.10	0.72 ± 0.13
	1.0	2231.82 ± 0.13	0.78 ± 0.19
IB	0.10	771.82 ± 0.01	0.35 ± 0.29
	0.25	1073.75 ± 0.23	0.53 ± 0.12
	0.5	1837.04 ± 0.15	0.73 ± 0.09
	1.0	2416.98 ± 0.17	0.79 ± 0.13
IFM	0.10	948.46 ± 0.15	0.47 ± 0.17
	0.25	1425.85 ± 0.21	0.65 ± 0.12
	0.50	1852.39 ± 0.12	0.73 ± 0.11
	1.0	2453.07 ± 0.09	0.80 ± 0.13
IF	0.10	1198.87 ± 0.03	0.58 ± 0.19
	0.25	1567.30 ± 0.02	0.68 ± 0.11
	0.50	2237.46 ± 0.09	0.78 ± 0.05
	1.0	2634.88 ± 0.09	0.81 ± 0.12

C_{Inh}: corrosion inhibitor concentration; R_P: polarization resistance; θ: surface coverage; IM: imidazole; IA: 4-(1*H*-imidazol-1-yl)aniline; IB: 4-(1*H*-imidazol-1-yl)benzaldehyde; IF: 4-(1*H*-imidazol-1-yl)phenol; IFM: (4-(1*H*-imidazol-1-yl)phenyl)methanol.

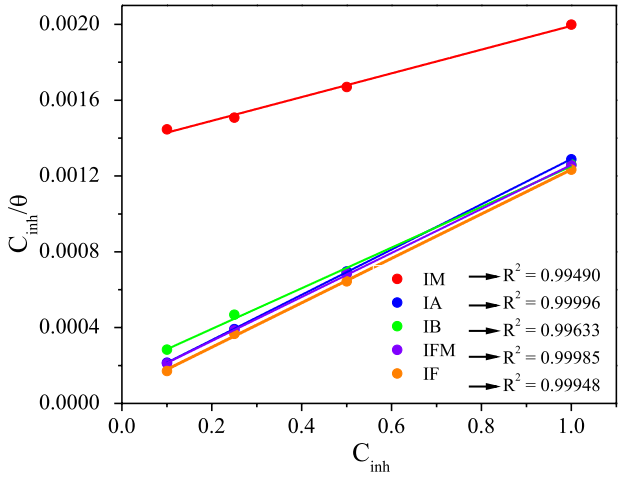

Figure 7. Langmuir's linear relationships obtained for the corrosion inhibition of Cu^0 in 0.5 mol L^{-1} H_2SO_4 solution in presence of imidazole and imidazole-based compounds.

lateral attractive interactions helps creating a protective layer of corrosion inhibitor molecule, the Frumkin isotherm suggest that the IM molecule is not an efficient corrosion

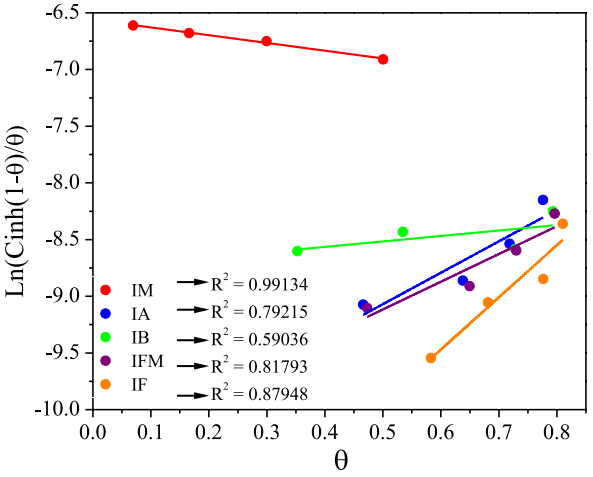

Figure 8. Frumkin adsorption isotherms plots obtained for imidazole and its derivatives.

Table 4. Intermolecular factors obtained from linearized Frumkin isotherm plots shown in Figure 8 for lateral groups of the studied molecule inhibitors for copper in H_2SO_4 0.5 mol L^{-1} solution

Molecule	Intermolecular factor (b)	Lateral group
IM	–0.68	
IA	2.77	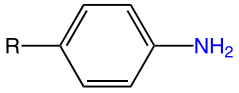
IB	0.48	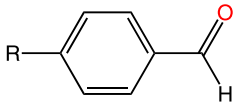
IFM	2.45	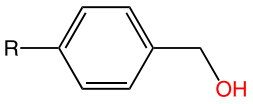
IF	4.60	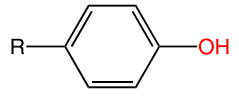

IM: imidazole; IA: 4-(1*H*-imidazol-1-yl)aniline; IB: 4-(1*H*-imidazol-1-yl) benzaldehyde; IF: 4-(1*H*-imidazol-1-yl)phenol; IFM: (4-(1*H*-imidazol-1-yl)phenyl)methanol.

inhibitor for Cu^0 in acidic medium due to the repulsion forces between the IM molecules adsorbed on Cu^0 surface.

For comparison with other isotherms, a Temkin isotherm model was applied by using equation 25, and the results are presented in Figure 9. In equation 25, B is related to the heat of adsorption, while K_f is the Temkin adsorption constant. In Figure 9, the Temkin adsorption isotherms, in a qualitative way, showed to be like the Frumkin isotherms in Figure 8: the IFM and IA isotherms were close one to another, but except IB isotherm the other isotherms were parallel. Also, the R^2 values were all greater than 0.9, which means that a strong linear correlation was achieved. Since there is a consideration of the adsorbent-adsorbent

interactions, but the adsorption enthalpy decreases when the surface coverage increases. In this context, the IF isotherm had the most surface recover than other molecules, confirming its better corrosion protection towards copper electrode.

$$\theta = B\ln K_f + B\ln C_{Inh} \quad (25)$$

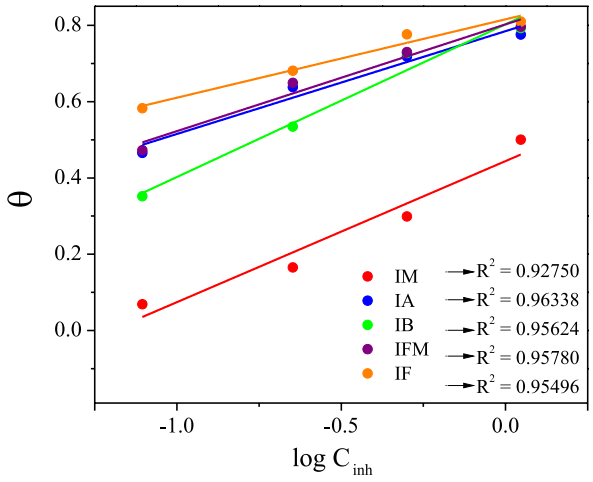

Figure 9. Temkin adsorption isotherms plots obtained for imidazole and its derivatives.

From the data obtained from the Langmuir and Frumkin isotherms, it was possible to obtain K_{ads} and, consequently, the free adsorption energy (ΔG_{ads}) of the compounds under study, by equation 26. In this equation, ΔG_{ads} is the adsorption energy, R is the real gas constant and T is the temperature in Kelvin.[73] Finally, the computed data for both isotherm models are displayed in Table 5.

$$\Delta G_{ads} = -RT\ln(55.6 \times K_{ads}) \quad (26)$$

The data displayed in Table 5 show that the Langmuir model fits better the experimental results of the Cu^0 corrosion inhibition in acid medium by the tested imidazole-based compounds, since the K_{ads} value increases and the ΔG_{ads} value shifts to more negative values in the same order of the ε_{inh} (Tables 1 and 2), while for the Frumkin model the order was not followed. In addition, the negative ΔG_{ads} values ensures that the adsorption of inhibitors is a spontaneous process forming a stable layer. Moreover, it is known that ΔG_{ads} values around –20 kJ mol^{-1} are generally attributed to physisorption of the inhibitor molecule on the metal surface, which is attributed to the electrostatic interactions between molecules and the electrode surface, while values more around than –30 kJ mol^{-1}, are attributed to adsorption by chemisorption, that is, to the electronic transfer between the molecules and the surface and, consequently, creating a chemical bond.[14] Therefore, correlating ΔG_{ads} (Table 5)

Table 5. K_{ads} and ΔG_{ads} values for imidazole derivatives in 0.5 mol L^{-1} H_2SO_4 solution for Cu^0 surface

Molecule	K_{ads} [a] (Langmuir)	ΔG_{ads} [b] (Langmuir) / (kJ mol^{-1})	K_{ads} [c] (Frumkin)	ΔG_{ads} [d] (Frumkin) / (kJ mol^{-1})
IM	7.30×10^2	–26.29	7.06×10^2	–26.21
IA	3.94×10^3	–30.47	3.45×10^4	–35.85
IB	5.60×10^3	–31.34	6.37×10^3	–31.66
IFM	1.03×10^3	–32.85	3.10×10^4	–35.57
IF	1.61×10^4	–33.96	2.05×10^5	–40.26

[a]Adsorption constant from Langmuir isotherm model; [b]Gibbs energy from Langmuir isotherm model; [c]adsorption constant from Frumkin isotherm model; [d]Gibbs energy from Frumkin isotherm moldel. IM: imidazole; IA: 4-(1*H*-imidazol-1-yl)aniline; IB: 4-(1*H*-imidazol-1-yl)benzaldehyde; IF: 4-(1*H*-imidazol-1-yl)phenol; IFM: (4-(1*H*-imidazol-1-yl)phenyl) methanol.

with the ε_{inh} (Tables 1 and 3), it is possible to note that the ε_{inh} increase with the increase of the chemical character of the interaction between the corrosion inhibitor molecule with the Cu^0 surface.

Computational results

The quantum chemical calculations were used to understand the charge transfer process between the candidate molecules for corrosion inhibitors in this work and the Cu^0 metallic surface. In Figure 10, the optimized structures in water (implicit solvent) are shown using the M06-2X/6-311++G(d,p) computational level for molecules that are candidates for corrosion inhibitors. The simulated molecular structures are not entirely planar, as the aromatic ring is not in the same plane as the imidazole ring. The functional M06-2X predicted similar values for the dihedral angle between the aromatic ring and the imidazole ring: 47.47° (IA), 45.16° (IB), 49.79° (IF), and 46.69° (IFM). Structurally, the only difference between these molecules is the functional group bonded in the aromatic ring and the charge value, since the acidic medium was used in the experimental tests, these molecules are in a protonated state according to the methodology used in previous work of the research group.[74]

Then, from the optimized structure of these molecules, the frontier molecular orbitals (HOMO and LUMO) were computed at the same level of theory, as well as the energy values of these molecular orbitals. Figure 11 shows the isosurfaces rendered for the HOMO and LUMO of the title molecules of this work. For the IA molecule, HOMO is mainly spread over the aromatic and imidazole rings, while LUMO is spread over the π* anti-ligand positions in the aromatic and imidazole rings. There is only a small contribution to the HOMO of the amine (protonated)

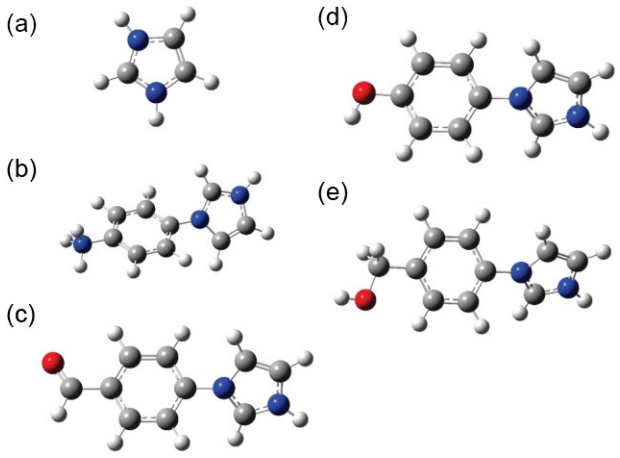

Figure 10. Optimized molecular geometry of the IM (a), IA (b), IB (c), IF (d), and IFM (e) obtained at M06-2X/6-311++G(d,p) level of theory in water as implicit solvent.

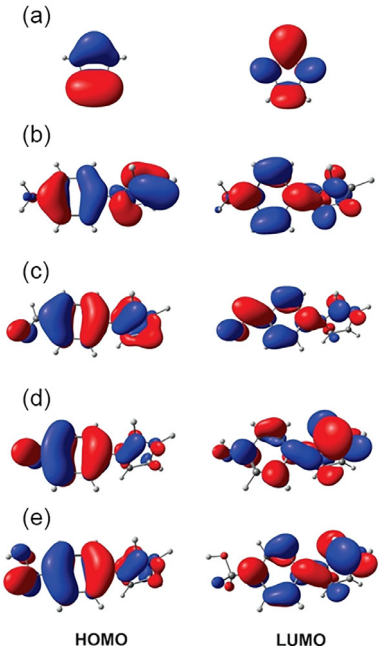

Figure 11. Frontier molecular orbitals calculated at M06-2X/6-311++G(d,p) level of theory in water for the molecules IM (a), IA (b), IB (c), IF (d), and IFM (e) with isovalue = 0.03.

group. For the IB molecule, HOMO is spread similarly to the IA molecule, however, there is a lower probability density spread over the imidazole ring in the IB molecule compared to the IA. It is possible to see an increase in the contribution of the functional group of the molecule IB (carbonyl group) compared to the amine group present in the molecule IA. This fact shows that there is a change in the reactivity site between the IB and IA molecules. For the IF and IFM molecules, the distribution of HOMO is like the isosurfaces spread mainly over the aromatic ring and in the functional groups, phenol, and methoxy, respectively. LUMO also shows to have a similar probability distribution for these two molecules, the electronic density is mainly spread over the π^* antibonding positions in the aromatic and imidazole rings, however, there is an increase in the probability density in the imidazole ring of these two molecules when compared to the IA and IB molecules that have a higher electronic density in the aromatic ring for LUMO.

From the analysis of the frontier molecular orbitals, it is already possible to notice the differences in the reactive sites of the title molecules of this work, while IA and IB show a greater probability of interaction with the metallic Cu^0 surface using the imidazole ring to donate electronic density and the aromatic ring to receive via retro-donation from the metallic surface. In the case of the IF and IFM molecules, the donation of electronic density is more probable using the aromatic ring, since the acceptance of charge coming from Cu^0, is more propensity to occur in the imidazole ring.

As the differences occur in the electronic properties, from the energy values of HOMO and LUMO, the quantum reactivity descriptors for the molecules of interest in this work were calculated and the results are shown in Table 6. The HOMO is related to the nucleophilic power of the molecule, since the higher the energy of this molecular orbital, the higher the propensity to donate electronic density. The LUMO is related to electrophilic power since the lower the energy value, the higher the propensity of the molecule to receive extra electronic density. Analyzing the data obtained in Table 6, it is possible to see that the HOMO energy values for the IA and IB molecules are close when compared to the imidazole molecule, with IB showing a greater difference of approximately 0.3 eV and IA of only 0.017 eV. As stated earlier, the probability density in the imidazole ring is greater than that of the aromatic ring for IA and IB, so when these molecules interact with metallic Cu^0, it is to be expected that the spatial arrangement of these molecules has the imidazole ring preferably facing the metallic surface. The IF and IFM molecules have higher HOMO energy values, which show greater reactivity when the interaction site is the aromatic ring compared to the imidazole ring. This trend is confirmed by the ionization potential (IP), which is related to the energy of HOMO and the nucleophilicity index (ε), hence the IF and IFM molecules, when compared to IA, IB, and the imidazole, has a greater tendency to donate electronic density.

The results for the LUMO energy values show that the IA and IB molecules are more likely to receive electronic density since they have the lowest energy values within the set of the five molecules. For these two molecules, the electronic density is more likely to spread over the empty

molecular orbitals in the aromatic ring, which again shows a greater reactivity when compared to the imidazole ring. The IF and IFM molecules also have lower LUMO values than imidazole since they can accommodate the extra negative charge density better than imidazole. This trend is also in agreement with the quantum descriptors such as the electronic affinity (A) and the electrophilicity index (ω). Therefore, according to the frontier molecular orbitals, it is noted that the IA and IB molecules have higher electrophilic character, whereas the IF and IFM molecules have higher nucleophilic character. Therefore, these molecules should interact differently with metallic Cu^0.

Another way to evaluate reactivity is through the energy gap between HOMO and LUMO. When this quantum descriptor is used, both nucleophilic and electrophilic characters are considered, since a smaller value of the energy gap implies a greater propensity to donate and accept electronic density, which confirms greater reactivity. According to the calculated results, the increasing order of the energy gap is IB < IF < IFM < IA < IM. This trend is the same as that obtained for the descriptors of global hardness and softness. Since a metallic bulk is classified as soft, as the IB molecule has the lowest hardness (greatest softness), it is expected to be the most reactive when considering only the energy gap. However, the order of corrosion inhibition found by the theoretical energy gap was practically the opposite of the experimentally predicted order. The data suggest that as the energy gap considers both the nucleophilic and electrophilic character of the molecules, it was seen that the availability of the LUMO cannot predict a correct order, but only the HOMO, so the energy gap is not a suitable quantum descriptor of reactivity to raking these molecules as corrosion inhibition of Cu^0 in acidic media.

Finally, using the quantum descriptors of electronegativity (χ) and the fraction of electrons transferred (ΔN), it is possible to evaluate how the charge transfer process occurs between the organic molecule and the Cu^0 metallic surface. Molecules IA and IB have greater electronegativity than the metallic surface, so the natural direction of the charge flow will be from Cu^0 to the molecule (ΔN < 0), as previously discussed showing the greater electrophilic character of these two molecules. The IF and IFM molecules, on the other hand, have less electronegativity than metallic Cu, so the charge flow will be from the molecule to the metal (ΔN > 0), thus showing the greater nucleophilic character discussed in the HOMO analysis. Therefore, it can be concluded that the action of these organic molecules as corrosion inhibitors is mainly due to the acceptance of electronic density (IA and IB) and the donation of electronic density (IF and IFM). All these imidazole derivatives have great potential to act as corrosion inhibitors, with the IB, IF and IFM molecules having greater corrosion efficiencies than the IA molecule since, within the four derivatives, it is the molecule that is least likely to interact with Cu^0.

It is possible to see in Figure 12 that the calculated isosurfaces for the title molecules show both the probability of donation (HOMO) and acceptance (LUMO) of electronic density. However, a greater understanding of the local reactivity of these molecules is necessary so that it is possible to recognize the trends presented in the global quantum reactivity descriptors. In this context, electronic Fukui functions were calculated based on the electronic density calculated for these molecules and the isosurfaces are shown in Figure 12. The green colored isosurfaces mean positive values of the Fukui functions and those with blue color represent negative values. The

Table 6. Global quantum reactivity descriptors computed for the molecules IM, IA, IB, IF, and IFM at M06-2X/6-311++G(d,p) level of theory

	IM	IA	IB	IF	IFM
HOMO energy (E_{HOMO}) / eV	–9.519	–9.502	–9.182	–8.273	–8.623
LUMO energy (E_{LUMO}) / eV	–0.103	–1.185	–1.660	–0.540	–0.683
Energy gap (ΔE_{gap}) / eV	9.417	8.317	7.521	7.734	7.940
Ionization potential (IP) / eV	9.519	9.502	9.182	8.273	8.623
Electron affinity (A) / eV	0.103	1.185	1.660	0.540	0.683
Electronegativity (χ) / eV	4.811	5.343	5.421	4.406	4.653
Global hardness (η) / eV	4.708	4.159	3.761	3.867	3.970
Global softness (σ) / eV^{-1}	0.212	0.240	0.266	0.259	0.252
Electrophilicity index (ω) / eV	2.458	3.433	3.907	2.511	2.727
Nucleophilicity index (ε) / eV^{-1}	0.407	0.291	0.256	0.398	0.367
Fraction of electrons transferred (ΔN)	0.018	–0.044	–0.059	0.074	0.041

IM: imidazole; IA: 4-(1*H*-imidazol-1-yl)aniline; IB: 4-(1*H*-imidazol-1-yl)benzaldehyde; IF: 4-(1*H*-imidazol-1-yl)phenol; IFM: (4-(1*H*-imidazol-1-yl) phenyl)methanol.

greater the value of the Fukui function, the greater the probability that the molecule will suffer a nucleophilic (f^+) or electrophilic (f^-).

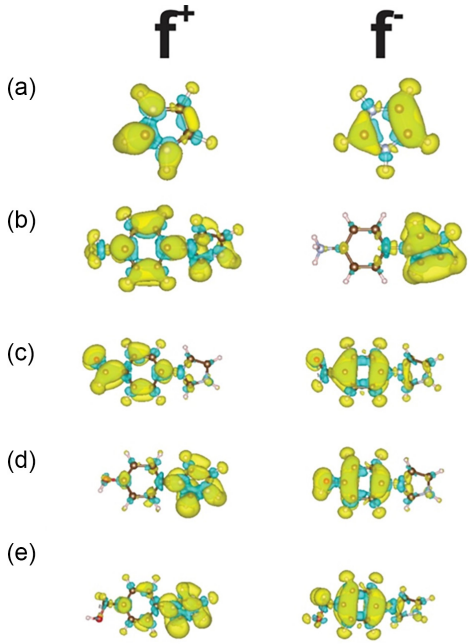

Figure 12. Isosurfaces for the electronic Fukui functions for nucleophilic (f^+) and electrophilic (f^-) attack for the molecules IM (a), IA (b), IB (c), IF (d), and IFM (e) with isovalue = 0.36.

For a nucleophilic attack (the molecule acts as an electrophilic site), the IA molecule has positive values of f^+ function in atoms in the aromatic ring and in the imidazole ring. The IB molecule has positive values predominantly in the aromatic ring and the carbonyl group. The IF and IFM molecules have the distribution of the f^+ function similar with the positive values mostly distributed in the imidazole ring. The IA and IB molecules have a greater electrophilic character because they are more likely to accept electronic density, with the IB molecule being more propensity to stabilize this extra negative charge because of the oxygen atom. The IF and IFM molecules could also have a high electrophilic character, however, it is in the imidazole ring that the electrophilic interaction site resides, so the negative charge cannot be spread efficiently.

For the electrophilic attack (the molecule acts as a nucleophilic site), the IA molecule presents positive values of the Fukui function in the imidazole ring, whereas the IB, IF and IFM molecules have positive values mainly in the aromatic ring and the oxygenated functional group. This result shows that these three molecules have a similar way of donating electronic density, but with greater effectiveness in the stabilization by the resonance effect in the IB molecule, IF and IFM have a greater nucleophilic character as previously predicted.

To finalize the local analysis of reactivity, the molecular electrostatic potential was calculated for molecules at the same level of theory as the frontier molecular orbitals and the results are shown in Figure 13. The region colored in red represents negative charges, the region-colored orange to yellow represents partially negative charges, the region in green represents charges tending to neutrality, the region in light blue, partially positive charges, and the dark blue region positive charges. It is possible to note that the IA molecule has a partial positive charge on the hydrogen atoms attached to the nitrogen atoms, and in the aromatic and imidazole rings the charge density is well distributed, showing that among the four molecules derived from imidazole, it must be the least reactive. The IB, IF and IFM molecules have a similar charge distribution. The three have a partially positive charge on the imidazole ring, a partially negative charge distributed on the aromatic ring, showing that it is in fact a site for the donation of electronic density and a negative charge on the oxygen atoms of the functional groups. This result shows agreement between what has been said about the frontier molecular orbitals and the electronic Fukui functions.

From the results of the adsorption Gibbs energy (ΔG_{ads}) using the Langmuir isotherm, the increase of adsorption energy follows the same tendency as the electronic density donation power using the HOMO energy value (IM < IA < IB < IFM < IF). According to the HOMO energy value (Table 6), the IF, IFM, and IB molecules have a higher value

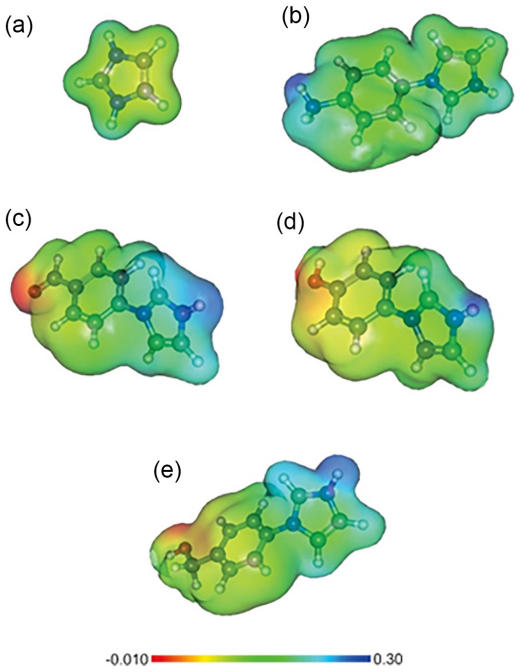

Figure 13. Molecular electrostatic potential computed for the molecules IM (a), IA (b), IB (c), IF (d), and IFM (e) at M06-2X/6-311++G(d,p) level of theory in water with isovalue = 0.01.

for the energy for this molecular orbital, which implies a higher tendency to donate the electronic density to the Cu^0 surface. Even though the FMO distribution (Figure 11) showed that the IA molecule has an electronic density in the benzene ring that can be donated, however, the electronic Fukui function (Figure 12) for the electrophilicity attack (f^-) demonstrated that the probability of the electronic density donation using the benzene ring for the IA molecule is almost nonexistent. Hence, for the IA molecule, the interaction with the Cu^0 surface should occur using the imidazole ring and this fact can be seen in the adsorption isotherms since the ΔG_{ads} is higher considering all the derivates.

For the IF, IFM, and IB molecules, the donation of the electronic density should occur using the benzene ring as showed the isosurfaces of the electronic Fukui functions. The IF molecule can interact using both the π electronic density spread over the benzene ring and the electronic density in the hydroxyl group. The IFM molecule can use the electronic density spread over in the aromatic ring and in the methoxy group to donate electrons to the Cu^0. However, it has a lower probability compared with the hydroxyl group of the IF molecule. The IB molecule can use besides the aromatic ring, the electronic density in the carbonyl group, however, the delocalization effect decreases the probability of electronic donation to the Cu^0 surface, and this molecule should have the higher ΔG_{ads} from these three sets of derivates (IF, IFM, and IB). The MEP distribution (Figure 13) also corroborates with the previous results due to the increase of the yellow-colored region over the aromatic ring for the IB, IFM, and IF molecules. Hence the charge available to be donated to the Cu^0 surface is higher for the IF molecule, which explains the lowest value for the ΔG_{ads} for this molecule.

Conclusions

The electrochemical corrosion tests demonstrated that the investigated imidazole derivative molecules inhibit the Cu^0 corrosion in acid medium in the following sequence: IF > IFM > IB > IA > IM. The adsorption data demonstrated that the Langmuir model fit better the experimental inhibition efficiency than the Frumkin model isotherms. Furthermore, the correlation between the ΔG_{ads} values and ε_{inh} values showed that the last increased with the chemical character of the interaction between the corrosion inhibitor molecules with the Cu^0 surface. The different DFT functions did not significantly change the molecular data, but global hardness of the modified molecules was different in comparison with imidazole molecule, since the chemical groups brings more chemical information and better corrosion inhibition efficiency. Since then, the Fukui analysis showed that modified imidazole modified molecules presented a higher electrophilic behavior, which could be accepted as a good capacity of receiving the electron density from Cu^0 electrode. In this context, the harmonic correlation of computational and experimental data led to successfully show the chemical modification of imidazole molecules for better anticorrosion efficiency in acidic media towards the protection of Cu^0 surfaces.

Acknowledgments

The authors thank the financial support given by the following Brazilian funding agencies: Coordenação de Aperfeiçoamento de Pessoal de Nível Superior (CAPES), Conselho Nacional de Desenvolvimento Científico e Tecnológico (CNPq) and Fundação Cearense de Apoio ao Desenvolvimento Científico e Tecnológica (FUNCAP). Stefane N. Costa and Francisco W. Q. Almeida-Neto thanks FUNCAP and CNPq for their scholarships. Pedro de Lima-Neto thanks the financial support received from CNPq projects 408626/2018-6 and 304152/2018-8. Adriana N. Correia thanks financial support received from CNPq projects: 305136/2018-6 and 405596/2018-9. The authors also thanks Centro Nacional de Processamento de Alto Desempenho (CENAPAD) of the Federal University of Ceará (UFC) for providing computational resources.

Author Contributions

Stefane N. Costa was responsible for data curation, formal analysis, methodology, investigation, writing - original draft, writing - review and editing, validation, visualization; Francisco W. Q. Almeida-Neto for formal analysis, investigation, writing - review and editing, validation, visualization; Emmanuel S. Marinho for data curation, formal analysis. supervision, validation, writing - review and editing; Othon S. Campos for data curation, formal analysis, supervision, project administration, investigation, writing - original draft, writing - review and editing, validation, visualization; Adriana Nunes Correia for funding acquisition, resources, supervision, investigation, writing - review and editing; Pedro de Lima Neto for conceptualization, data curation, formal analysis, funding acquisition, methodology, project administration, resources, supervision, validation, visualization, writing - original draft, writing - review and editing.

References

1. Abdulazeez, I.; Zeino, A.; Kee, C. W.; Al-Saadi, A. A.; Khaled, M.; Wong, M. W.; Al-Sunaidi, A. A.; *Appl. Surf. Sci.* **2019**, *471*, 494. [Crossref]
2. El-katori, E. E.; Abousalem, A. S.; *RSC Adv.* **2019**, *9*, 20760. [Crossref]

3. Dagdag, O.; Safi, Z.; Wazzan, N.; Erramli, H.; Guo, L.; Mkadmh, A. M.; Verma, C.; Ebenso, E. E.; El Gana, L.; El Harfi, A.; *J. Mol. Liq.* **2020**, *302*, 112535. [Crossref]
4. Chaouiki, A.; Lgaz, H.; Salghi, R.; Gaonkar, S. L.; Bhat, K. S.; Jodeh, S.; Toumiat, K.; Oudda, H.; *Port. Electrochim. Acta* **2019**, *37*, 147. [Crossref]
5. Arkhipushkin, I. A.; Agafonkina, M. O.; Kazansky, L. P.; Kuznetsov, Y. I.; Shikhaliev, K. S.; *Electrochim. Acta* **2019**, *308*, 392. [Crossref]
6. Huang, H.; Bu, F.; *Corros. Sci.* **2020**, *165*, 108413. [Crossref]
7. Burke, K.; Perdew, J. P.; Wang, Y.; *Electronic Density Functional Theory*; Springer US: Boston, MA, 1998.
8. Hamadi, L.; Mansouri, S.; Oulmi, K.; Kareche, A.; *Egypt. J. Pet.* **2018**, *27*, 1157. [Crossref]
9. Farahati, R.; Ghaffarinejad, A.; Mousavi-Khoshdel, S. M.; Rezania, J.; Behzadi, H.; Shockravi, A.; *Prog. Org. Coat.* **2019**, *132*, 417. [Crossref]
10. Xu, Y.; Zhang, S.; Li, W.; Guo, L.; Xu, S.; Feng, L.; Madkour, L. H.; *Appl. Surf. Sci.* **2018**, *459*, 612. [Crossref]
11. Zhang, Y.; Zhu, H.; Zhuang, C.; Chen, S.; Wang, L.; Dong, L.; Yin, Y.; *Mater. Chem. Phys.* **2016**, *179*, 80. [Crossref]
12. Kovačević, N.; Milošev, I.; Kokalj, A.; *Corros. Sci.* **2015**, *98*, 457. [Crossref]
13. El Ibrahimi, B.; Soumoue, A.; Jmiai, A.; Bourzi, H.; Oukhrib, R.; El Mouaden, K.; El Issami, S.; Bazzi, L.; *J. Mol. Struct.* **2016**, *1125*, 93. [Crossref]
14. Qiang, Y.; Zhang, S.; Yan, S.; Zou, X.; Chen, S.; *Corros. Sci.* **2017**, *126*, 295. [Crossref]
15. Dagdag, O.; El Harfi, A.; Safi, Z.; Guo, L.; Kaya, S.; Verma, C.; Ebenso, E. E.; Wazzan, N.; Quraishi, M. A.; El Bachiri, A.; El Gouri, M.; *J. Mol. Liq.* **2020**, *308*, 113020. [Crossref]
16. Qiang, Y.; Zhang, S.; Wang, L.; *Appl. Surf. Sci.* **2019**, *492*, 228. [Crossref]
17. Marinescu, M.; *BMC Chem.* **2019**, *13*, 136. [Crossref]
18. Lourenço, M. P.; Anastácio, A. S.; Rosa, A. L.; Frauenheim, T.; da Silva, M. C.; *J. Mol. Model.* **2020**, *26*, 187. [Crossref]
19. Njoku, D. I.; Oguzie, E. E.; Li, Y.; *J. Mol. Liq.* **2017**, *237*, 247. [Crossref]
20. Chaouiki, A.; Lgaz, H.; Chung, I. M.; Ali, I. H.; Gaonkar, S. L.; Bhat, K. S.; Salghi, R.; Oudda, H.; Khan, M. I.; *J. Mol. Liq.* **2018**, *266*, 603. [Crossref]
21. Dennington, R.; Keith, T.; Millam, J.; *GaussView*, v. 5.0.8; Semichem Inc., United States, 2003.
22. Frisch, M. J.; Trucks, G. W.; Schlegel, H. B.; Scuseria, G. E.; Robb, M. A.; Cheeseman, J. R.; Scalmani, G.; Barone, V.; Petersson, G. A.; Nakatsuji, H.; Li, X.; Caricato, M.; Marenich, A. V.; Bloino, J.; Janesko, B. G.; Gomperts, R.; Mennucci, B.; Hratchian, H. P.; Ortiz, J. V.; Izmaylov, A. F.; Sonnenberg, J. L.; Williams; Ding, F.; Lipparini, F.; Egidi, F.; Goings, J.; Peng, B.; Petrone, A.; Henderson, T.; Ranasinghe, D.; Zakrzewski, V. G.; Gao, J.; Rega, N.; Zheng, G.; Liang, W.; Hada, M.; Ehara, M.; Toyota, K.; Fukuda, R.; Hasegawa, J.; Ishida, M.; Nakajima, T.; Honda, Y.; Kitao, O.; Nakai, H.; Vreven, T.; Throssell, K.; Montgomery Jr., J. A.; Peralta, J. E.; Ogliaro, F.; Bearpark, M. J.; Heyd, J. J.; Brothers, E. N.; Kudin, K. N.; Staroverov, V. N.; Keith, T. A.; Kobayashi, R.; Normand, J.; Raghavachari, K.; Rendell, A. P.; Burant, J. C.; Iyengar, S. S.; Tomasi, J.; Cossi, M.; Millam, J. M.; Klene, M.; Adamo, C.; Cammi, R.; Ochterski, J. W.; Martin, R. L.; Morokuma, K.; Farkas, O.; Foresman, J. B.; Fox, D. J.; *Gaussian 09 Rev. B.01*, Wallingford, CT, year.
23. Ditchfield, R.; Hehre, W. J.; Pople, J. A.; *J. Chem. Phys.* **1971**, *54*, 724. [Crossref]
24. Zhao, Y.; Truhlar, D. G.; *Theor. Chem. Acc.* **2008**, *120*, 215. [Crossref]
25. Mennucci, B.; Cancès, E.; Tomasi, J.; *J. Phys. Chem. B* **1997**, *101*, 10506. [Crossref]
26. Cancès, E.; Mennucci, B.; Tomasi, J.; *J. Chem. Phys.* **1997**, *107*, 3032. [Crossref]
27. Zhurko, G. A.; *Chemcraft*, version 1.8; Chemcraft Corp., Russia, 2014.
28. Pearson, R. G.; *J. Am. Chem. Soc.* **1963**, *85*, 3533. [Crossref]
29. Koopmans, T.; *Physica* **1934**, *1*, 104. [Crossref]
30. Chermette, H.; *J. Comput. Chem.* **1999**, *20*, 129. [Crossref]
31. Iczkowski, R. P.; Margrave, J. L.; *J. Am. Chem. Soc.* **1961**, *83*, 3547. [Crossref]
32. Pearson, R. G.; *J. Chem. Educ.* **1987**, *64*, 561. [Crossref]
33. Janak, J. F.; *Phys. Rev. B* **1978**, *18*, 7165. [Crossref]
34. Von Szentpály, L.; *J. Mol. Struct. THEOCHEM* **1991**, *233*, 71. [Crossref]
35. Yang, W.; Parr, R. G.; *Proc. Natl. Acad. Sci.* **1985**, *82*, 6723. [Crossref]
36. Parr, R. G.; Szentpály, L. V.; Liu, S.; *J. Am. Chem. Soc.* **1999**, *121*, 1922. [Crossref]
37. Chattaraj, P. K.; Giri, S.; Duley, S.; *Chem. Rev.* **2011**, *111*, PR43. [Crossref]
38. Obot, I. B.; Macdonald, D. D.; Gasem, Z. M.; *Corros. Sci.* **2015**, *99*, 1. [Crossref]
39. Dewar, M. J. S.; Zoebisch, E. G.; Healy, E. F.; Stewart, J. J. P.; *J. Am. Chem. Soc.* **1985**, *107*, 3902. [Crossref]
40. Michaelson, H. B.; *J. Appl. Phys.* **1977**, *48*, 4729. [Crossref]
41. Lu, T.; Chen, F.; *J. Comput. Chem.* **2012**, *33*, 580. [Crossref]
42. Momma, K.; Izumi, F.; *J. Appl. Crystallogr.* **2011**, *44*, 1272. [Crossref]
43. Allouche, A.-R.; *J. Comput. Chem.* **2011**, *32*, 174. [Crossref]
44. Mihajlović, M. B. P.; Radovanović, M. B.; Tasić, Ž. Z.; Antonijević, M. M.; *J. Mol. Liq.* **2017**, *225*, 127. [Crossref]
45. Dhouibi, I.; Masmoudi, F.; Bouaziz, M.; Masmoudi, M.; *Arabian J. Chem.* **2021**, *14*, 102961. [Crossref]
46. Tan, B.; Zhang, S.; Liu, H.; Qiang, Y.; Li, W.; Guo, L.; Chen, S.; *J. Taiwan Inst. Chem. Eng.* **2019**, *102*, 424. [Crossref]

47. Jmiai, A.; el Ibrahimi, B.; Tara, A.; Chadili, M.; El Issami, S.; Jbara, O.; Khallaayoun, A.; Bazzi, L.; *J. Mol. Liq.* **2018**, *268*, 102. [Crossref]
48. Zhou, L.; Zhang, S.; Tan, B.; Feng, L.; Xiang, B.; Chen, F.; Li, W.; Xiong, B.; Song, T.; *J. Taiwan Inst. Chem. Eng.* **2020**, *113*, 253. [Crossref]
49. Cordeiro, G. G. O.; Barcia, O. E.; Mattos, O. R.; *Electrochim. Acta* **1993**, *38*, 319. [Crossref]
50. Zhang, K.; Lu, J.; Li, J.; Zhang, D.; Gao, L.; Zhou, H.; *Corros. Sci.* **2020**, *164*, 108352. [Crossref]
51. Messali, M.; Larouj, M.; Lgaz, H.; Rezki, N.; Al-Blewi, F. F.; Aouad, M. R.; Chaouiki, A.; Salghi, R.; Chung, I. M.; *J. Mol. Struct.* **2018**, *1168*, 39. [Crossref]
52. Feng, L.; Zhang, S.; Qiang, Y.; Xu, Y.; Guo, L.; Madkour, L. H.; Chen, S.; *Materials (Basel)* **2018**, *11*, 1042. [Crossref]
53. Gao, L.; Peng, S.; Huang, X.; Gong, Z.; *Appl. Surf. Sci.* **2020**, *511*, 145446. [Crossref]
54. Feng, Y.; Feng, L.; Sun, Y.; He, J.; *J. Mater. Res. Technol.* **2020**, *9*, 584. [Crossref]
55. Tan, B.; Zhang, S.; Li, W.; Zuo, X.; Qiang, Y.; Xu, L.; Hao, J.; Chen, S.; *J. Ind. Eng. Chem.* **2019**, *77*, 449. [Crossref]
56. Tan, B.; Zhang, S.; Qiang, Y.; Guo, L.; Feng, L.; Liao, C.; Xu, Y.; Chen, S.; *J. Colloid Interface Sci.* **2018**, *526*, 268. [Crossref]
57. Gong, Z.; Peng, S.; Huang, X.; Gao, L.; *Materials (Basel)* **2018**, *11*, 2107. [Crossref]
58. Shi, C.; Wang, Y.; Yu, Y.; Li, J.; Zhang, D.; Gao, L.; *Corros. Sci.* **2018**, *145*, 100. [Crossref]
59. Li, H.; Zhang, S.; Tan, B.; Qiang, Y.; Li, W.; Chen, S.; Guo, L.; *J. Mol. Liq.* **2020**, *305*, 112789. [Crossref]
60. Bedrov, D.; Piquemal, J. P.; Borodin, O.; MacKerell Jr., A. D.; Roux, B.; Schröder, C.; *Chem. Rev.* **2019**, *119*, 7940. [Crossref]
61. Tan, B.; Zhang, S.; Qiang, Y.; Feng, L.; Liao, C.; Xu, Y.; Chen, S.; *J. Mol. Liq.* **2017**, *248*, 902. [Crossref]
62. Xu, B.; Ji, Y.; Zhang, X.; Jin, X.; Yang, W.; Chen, Y.; *J. Taiwan Inst. Chem. Eng.* **2015**, *51*, 193. [Crossref]
63. Mendonça, G. L. F.; Costa, S. N.; Freire, V. N.; Casciano, P. N. S.; Correia, A. N.; de Lima-Neto, P.; *Corros. Sci.* **2017**, *115*, 41. [Crossref]
64. Hsu, C. H.; Mansfeld, F.; *Corrosion* **2001**, *57*, 747. [Crossref]
65. Brug, G. J.; van den Eeden, A. L. G.; Sluyters-Rehbach, M.; Sluyters, J. H.; *J. Electroanal. Chem. Interfacial Electrochem.* **1984**, *176*, 275. [Crossref]
66. Luo, W.; Li, W.; Tan, J.; Liu, J.; Tan, B.; Zuo, X.; Wang, Z.; Zhang, X.; *J. Mol. Liq.* **2020**, *314*, 113630. [Crossref]
67. Orazem, M. E.; Tribollet, B.; *Electrochemical Impedance Spectroscopy*; John Wiley & Sons, Inc.: Hoboken, NJ, USA, 2008.
68. Chen, Z.; Xiaohui, J.; Cheng, Z.; Liao, Y.; Pu, Q.; Ming, D.; *Mater. Corros.* **2019**, *70*, 820. [Crossref]
69. Farahati, R.; Mousavi-Khoshdel, S. M.; Ghaffarinejad, A.; Behzadi, H.; *Prog. Org. Coat.* **2020**, *142*, 105567. [Crossref]
70. Quiroz, M.; Cordova, F.; Salgado, L.; Viniegra, M.; Meas, Y.; Díaz, G.; *Rev. Mex. Fis.* **1995**, *41*, 386. [Link]
71. Kolev, V. L.; Danov, K. D.; Kralchevsky, P. A.; Broze, G.; Mehreteab, A.; *Langmuir* **2002**, *18*, 9106. [Crossref]
72. Bastidas, D. M.; Gómez, R. R.; Cano, E.; *Rev. Metal.* **2005**, *41*, 98. [Crossref]
73. Corrales-Luna, M.; Le Manh, T.; Romero-Romo, M.; Palomar-Pardavé, M.; Arce-Estrada, E. M.; *Corros. Sci.* **2019**, *153*, 85. [Crossref]
74. Costa, S. N.; Almeida-Neto, F. W. Q.; Campos, O. S.; Fonseca, T. S.; de Mattos, M. C.; Freire, V. N.; Homem-de-Mello, P.; Marinho, E. S.; Monteiro, N. K. V.; Correia, A. N.; de Lima-Neto, P.; *J. Mol. Liq.* **2021**, *326*, 115330. [Crossref]

Submitted: April 14, 2022
Published online: August 16, 2022